

Winter Convective Mixing in the Northern Arabian Sea during Contrasting Monsoons

PRASAD G. THOPPIL,^a ALAN J. WALLCRAFT,^b AND TOMMY G. JENSEN^a

^a *Ocean Sciences Division, Naval Research Laboratory, Stennis Space Center, Mississippi*

^b *Center for Ocean-Atmospheric Prediction Studies, Florida State University, Tallahassee, Florida*

(Manuscript received 7 July 2021, in final form 6 December 2021)

ABSTRACT: Along-track Argo observations in the northern Arabian Sea during 2017–19 showed by far the most contrasting winter convective mixing; 2017–18 was characterized by less intense convective mixing resulting in a mixed layer depth of 110 m, while 2018–19 experienced strong and prolonged convective mixing with the mixed layer deepening to 150 m. The response of the mixed layer to contrasting atmospheric forcing and the associated formation of Arabian Sea High Salinity Water (ASHSW) in the northeastern Arabian Sea are studied using a combination of Argo float observations, gridded observations, a data assimilative general circulation model, and a series of 1D model simulations. The 1D model experiments show that the response of winter mixed layer to atmospheric forcing is not only influenced by winter surface buoyancy loss, but also by a preconditioned response to freshwater fluxes and associated buoyancy gain by the ocean during the summer that is preceding the following winter. A shallower and short-lived winter mixed layer occurred during 2017–18 following the exceptionally high precipitation over evaporation during the summer monsoon in 2017. The precipitation-induced salinity stratification (a salinity anomaly of -0.7 psu) during summer inhibited convective mixing in the following winter, resulting in a shallow winter mixed layer (103 m). Combined with weak buoyancy loss due to weaker surface heat loss in the northeastern Arabian Sea, this caused an early termination of the convective mixing (26 February 2018). In contrast, the winter convective mixing during 2018–19 was deeper (143 m) and long-lived. The 2018 summer, by comparison, was characterized by normal or below normal precipitation which generated a weakly stratified ocean preconditioned to winter mixing. This combined with colder and drier air from the landmass to the north with low specific humidity led to strong buoyancy loss, and resulted in prolonged winter convective mixing through 25 March 2019.


KEYWORDS: Indian Ocean; Atmosphere-ocean interaction; Buoyancy; Deep convection; Oceanic mixed layer; Water masses/storage

1. Introduction

In the northern Arabian Sea, excess evaporation over precipitation and surface heat loss (Prasad 1997; Kumar and Prasad 1999) during the boreal winter monsoon (November–February) lead to the convective formation of Arabian Sea High Salinity Water (ASHSW) (Prasad and Ikeda 2002a; Morrison 1997; Kumar and Prasad 1996; 1999; Prasad 1997; Rochford 1964). After formation in the northern Arabian Sea, it subsides in the region north of $\sim 20^\circ\text{N}$ and spreads equatorward along the $\sigma = 24$ isopycnal surface as a subsurface salinity maximum in the upper 100 m (Han et al. 2001; Prasad and Ikeda 2002b). The seasonally reversing monsoon circulation (Schott and McCreary 2001) modifies the spatio-temporal variability of the ASHSW and plays an important role in the salt budget of the Indian Ocean (Jensen 2003). The advection of low-salinity water from the Bay of Bengal by the North Equatorial Current (NEC) and its northward advection along the west coast of India by the West India Coastal Current (WICC; Shetye et al. 1991) contribute to the reduction in salinity during the boreal winter monsoon. At the same time, the southward flowing Somali Current (SC) advects high-

salinity water southward across the equator. During the boreal summer monsoon (June–September) the basin-scale circulation is clockwise. The northward flowing SC and currents along the coasts of Saudi Arabia and Oman reduces salinity through a combination of lateral mixing and vertical advection (Fischer et al. 2002; Bauer et al. 1991; Findlater 1969). At the same, the eastern flank of the basinwide circulation advects high-salinity ASHSW southward and subsequently eastward into the Bay of Bengal by the Indian Monsoon Current (IMC) and Wyrтки Jets (Jensen 2001; Schott and McCreary 2001; Wyrтки 1973).

A number of observational and numerical modeling studies have been conducted to investigate the processes at work during the formation and spreading of ASHSW (Kumar and Prasad 1996, 1999; Rochford 1964; Prasad and Ikeda 2002a,b; Joseph and Freeland 2005; Chowdary and Gnanaseelan 2005; Wang et al. 2013; Singh et al. 2019; Zhang et al. 2020). These studies demonstrated that both ocean dynamics and the atmospheric forcing can modulate the salinity variation in the Arabian Sea with short-term variability resulting from tropical cyclones (Wang et al. 2013) and mesoscale eddies (Zhang et al. 2020). In the northwestern Arabian Sea ocean dynamics play a major role in the modulation of ASHSW during the summer monsoon. The monsoon-driven circulation generates mesoscale eddies, coastal upwelling, fronts and coastal jets, and the Ras Al Hadd Jet (Flagg and Kim 1998; Böhm et al. 1999) and affects the spreading of ASHSW. In particular, Zhang et al. (2020) documented a prolonged high-salinity event in the

 Denotes content that is immediately available upon publication as open access.

Corresponding author: Prasad Thoppil, prasad.thoppil@nrlssc.navy.mil

DOI: 10.1175/JPO-D-21-0144.1

© 2022 American Meteorological Society. For information regarding reuse of this content and general copyright information, consult the AMS Copyright Policy (www.ametsoc.org/PUBSReuseLicenses).

northern Arabian Sea during 2014–17 which caused a significant positive salinity anomaly in the upper 400 m relative to the 2004–18 climatology. Due to the lack of strong correlation with evaporation, [Zhang et al. \(2020\)](#) attributed the high-salinity event to the seasonally dependent eddies near the mouth of the Gulf of Oman as a primary mechanism. The eddies appear to favor spreading of ASHSW to the northern Arabian Sea generating a persistent high-salinity event lasting three years (2014–17) as opposed to suppressing the spreading during the 2010–13 time frame. The anomalous eddies also intensified the eastward Ras Al Hadd Jet ([Flagg and Kim 1998](#)) causing the advection of high-salinity water into the northeastern Arabian Sea ([Zhang et al. 2020](#)). Unlike the northwestern Arabian Sea where ocean dynamics are dominant, the northeastern Arabian Sea is less prone to mesoscale eddies and strong currents. [Singh et al. \(2019\)](#) indicated buoyancy production of turbulent kinetic energy as the mechanism governing convective mixing and associated mixed layer variability in the northeastern Arabian Sea during the winter monsoon.

While formation of ASHSW is driven by convective mixing triggered by buoyancy loss from the ocean ([Prasad and Ikeda 2002a](#)), those processes are affected by the magnitude of surface cooling as well as the preconditioning of the ocean. In particular, what impact does the preconditioning of the ocean have on the evolution of convection? Here in this paper, we show that winter convective mixing is modulated by atmospheric forcing during contrasting monsoons, which are characterized by anomalous precipitation during the summer and anomalous evaporation in following winter. We find that the salinity-induced stratification triggered by excess precipitation during summer affects the following winter convective mixing and ASHSW formation in the northeastern Arabian Sea. The winter convective mixing preceded by a strong stratification was significantly shallower and short-lived than other years. By contrast, the convective mixing was deep and prolonged during the period of anomalous evaporation preceded by a weak stratification. We identified 2017–18 as an excess precipitation time span and 2018–19 as the time with the strongest evaporation. We attribute the contrasting mixed layer responses in the Argo float observations to the excess precipitation in the summer of 2017 followed by a period of weak buoyancy loss in the winter of 2017–18, and a period of deficient precipitation during the summer of 2018 followed by strong buoyancy loss in the 2018–19 winter. On the basis of mixed layer response to contrasting monsoons, we refer the 2017–18 as shallow convective mixing (SCM) and 2018–19 as deep convective mixing (DCM) periods. The period 2017–18 (2018–19) refers to May 2017–April 2018 (May 2018–April 2019) in the remainder of the paper. We employ a combination of observations and model simulations to identify and isolate the atmospheric forcing that lead to the contrasting winter convective mixing in the northeastern Arabian Sea.

The remainder of the paper is structured as follows. [Section 2](#) describes the observations and models utilized. The observational evidence for contrasting winter convective mixing is presented in [section 3a](#), followed by 1D model results in [section 3b](#). [Section 3c](#) identifies and isolates the processes affecting the

convective mixing using 1D model perturbation experiments. Contrasting atmospheric forcing is presented in [section 3d](#). Finally, the 2017–19 period is discussed in light of the interannual variability in [section 3e](#). Discussions and conclusions are given in [section 4](#).

2. Data and methods

a. Data

We used version 4 of the Met Office Hadley Centre series of datasets (EN4) of global quality-controlled ocean temperature and salinity profiles and monthly objective analyses. The dataset spans from 1900 to present and is based on subsurface ocean temperature and salinity profile data obtained from the World Ocean Database (WOD09; [Boyer et al. 2009](#)), Global Temperature and Salinity Profile Program (GTSP), Argo, and Arctic Synoptic Basin Wide Oceanography (ASBO) collections. Monthly potential temperature and salinity objective analyses were calculated from the quality-controlled ocean data. These have a regular $1^\circ \times 1^\circ$ horizontal grid and 42 levels in the vertical (see [Good et al. 2013](#) for details). This product provides a baseline of mixed layer depths and salinity for comparing with model results. We also used individual Argo float observations to identify contrasting convective mixing periods.

To delineate the atmospheric forcing that lead to the contrasting winter convective mixing, we used National Centers for Environmental Prediction (NCEP) Climate Forecast System Reanalysis (CFSR) data ([Saha et al. 2010](#)). The CFSR dataset consists of hourly weather forecasts generated by the National Weather Service's NCEP Global Forecast System. It should be noted that same dataset is used to force the 1D model described below.

b. Models

In the absence of eddy induced restratification by advection, convective mixing can be approximated as a one-dimensional (1D) process, where surface buoyancy loss triggers convection with the buoyancy loss being partly compensated by fluxes at the mixed layer base ([Prasad and Ikeda 2002a,b](#)). This assumption is not untenable to the process under study because [Prasad and Ikeda \(2002a\)](#) reproduced the winter convection and ASHSW formation in a 1D model. Here we use Hybrid Coordinate Ocean Model (HYCOM; [Bleck 2002](#)) configured as a one-dimensional model to simulate the upper-ocean response to contrasting atmospheric forcing. The *K*-profile parameterization (KPP; [Large et al. 1994](#)) vertical mixing scheme is used. While 1D models previously have been used to investigate the vertical mixing at a single point, HYCOM is configured for the Arabian Sea as a mesh of $1^\circ \times 1^\circ$ 1D models run independently at each grid point. This enabled us to compare between a 1D model, a 3D model, and the EN4. The 1D model is forced with NCEP CFSR hourly fields of wind stress, solar radiation, longwave radiation, specific humidity, air temperature, and precipitation. Model SST is used to calculate the surface heat flux. The model is initialized from the climatological temperature and salinity from

the Generalized Digital Environmental Model climatology (GDEM4; Carnes et al. 2010). For both the 2017–18 and 2018–19 periods, the model is reinitialized in May from GDEM4 temperature and salinity and integrated for a year (May–April) using realistic atmospheric forcing. There are 241 vertical layers with 1-m grid spacing in the upper 200 m, and the remaining 40 layers are distributed between 200 and 1000 m with variable grid spacing. As the deepest mixed layer during the period is shallower than 150 m, the coarse resolution below 200 m has negligible impact on the evolution of thermohaline properties.

The 1D model is complimented by results from a 1/12.5° Global Ocean Forecast System (GOFS), which is a global, three-dimensional (3D) HYCOM data assimilative system (Metzger et al. 2014). The GOFS consists of HYCOM for the ocean and the Navy Coupled Ocean Data Assimilation (NCODA), which uses a 3D variational data assimilation (3DVAR) method for assimilation of ocean and sea ice observations with a 24-h update cycle to constrain the mesoscale features to the available observations. The GOFS was initialized from GDEM, spun up, and validated against independent observations before being transitioned to become operational in early 2013. The operational GOFS uses atmospheric forcing from the operational Navy Global Environmental Model (NAVGEM). The details and specifics of the GOFS can be found in Metzger et al. (2010, 2014) and is not repeated here. The comparisons between 1D and 3D model results unravel the horizontal and vertical advection and lateral mixing processes that are not represented in a 1D model.

3. Results

a. Evolution of ASHSW during contrasting monsoons

Analysis of the Argo float observations obtained during the period 2017–19 revealed the presence of exceptionally different winter convective mixing depths. Figure 1 depicts the along-track evolution of salinity, temperature, and mixed layer depth (MLD) with geographical coordinates superimposed. The Argo float (ID 2903129), quasi-stationary in the region, drifted eastward between 19° and 22°N between May 2017 and February 2019, capturing contrasting winter convective mixing in the northeastern Arabian Sea with mixed layer depth differing 40 m. During 2018–19, the winter convective mixing was significantly stronger exceeding 150 m compared to 2017–18 (110 m). It should be noted that the longitudinal positions of the float during these winter monsoons differed by about 2°E at 21°N which may have accounted for part of the observed MLD differences. In response to winter buoyancy loss, the MLD started deepening in mid-October reaching its peak depth in January–February. Furthermore, the transition from a deep winter mixed layer to a shallow spring mixed layer (~30 m) between the periods were also different in the two cases. The transition occurred in early March 2018 while the deep winter mixed layer persisted through late March 2019 in the second year as is confirmed from EN4 (Argo observations ended in early March 2019). To further confirm the different winter convective mixing during the two

periods of Argo observations, we compared the mixed layer depth at a single point 22°N, 67°E from the EN4 gridded product of monthly mean temperature and salinity. As expected, the winter mixed layer depths during the periods were similar to those derived from the along-track Argo float observations (see open squares). Specifically, the transition from deep winter to shallow spring mixed layers was delayed by one month in the second year and occurred in April 2019. The mixed layer depth was different during August–September 2017 with a shallower MLD by ~30 m at 22°N, 67°E in EN4, possibly due to strong stratification induced by excess precipitation.

Associated with the convective mixing was the formation of ASHSW with salinity > 36.5 psu generating a vertically uniform salinity in the mixed layer from November through February. After formation, the ASHSW sinks and mixes with the water below as evidenced by high salinity of 36.5 psu in the 50–100 m depth range during May–August 2018. The ASHSW during the winter of 2018–19 was saltier than those in 2017–18, exceeding 36.8 psu, consistent with a stronger convective mixing. The mixed layer had a temperature of 24°–26°C during the periods of convective mixing due to winter heat loss albeit similar between the periods. The differences in salinity between the periods during the summer monsoon should be interpreted in the context of circulation relative to the float location. The presence of relatively fresher surface salinity between May and October 2017 can be associated with the location of the Argo float to the proximity to the western boundary currents. Coastal upwelling and offshore advection of low-salinity water (~21.7°N, ~61.1°E) caused a reduction in salinity (<36 psu) during June–July 2017 which is also evidenced by the upward heaving of the isotherms and associated surface cooling. As the float was confined to the area east of 65°E (~21.7°N) during the summer 2018, the basin-wide clockwise circulation advected ASHSW southward and exhibited a higher surface salinity. On the other hand, the salinity in the northern Arabian Sea during the winter monsoon was less prone to impact from the circulation and largely depended on the preconditioning of the water column and buoyancy loss.

To further explore the impact of winter convective mixing during contrasting monsoons on salinity, Fig. 2 shows salinity differences between 2019 and 2018 at 120 m for January–March from the EN4. Recall from Fig. 1 that convective mixing in these periods exhibit marked differences. Both products are consistent, showing higher salinity in 2019 than in 2018 with a peak difference of 0.5 psu in the northeastern Arabian Sea. This further confirms the increased production of ASHSW in 2019 from enhanced convective mixing particularly north of 20°N. During the restratification phase in March the upper-ocean gains heat from the atmosphere which marks the end of the convective period. Consequently, the newly formed ASHSW subducts and spreads laterally, mixing with ambient waters thereby reducing the salinity.

The salinity difference between the two winter periods is also reflected as significant anomalies from the long-term mean (2010–19). The winter salinity anomalies in excess of ± 0.1 psu are present in the northeastern Arabian Sea (65°–70°E, 20°–26°N) during the period 2017–19 (Fig. 3). The winter salinity of 2018–19 is characterized by above average

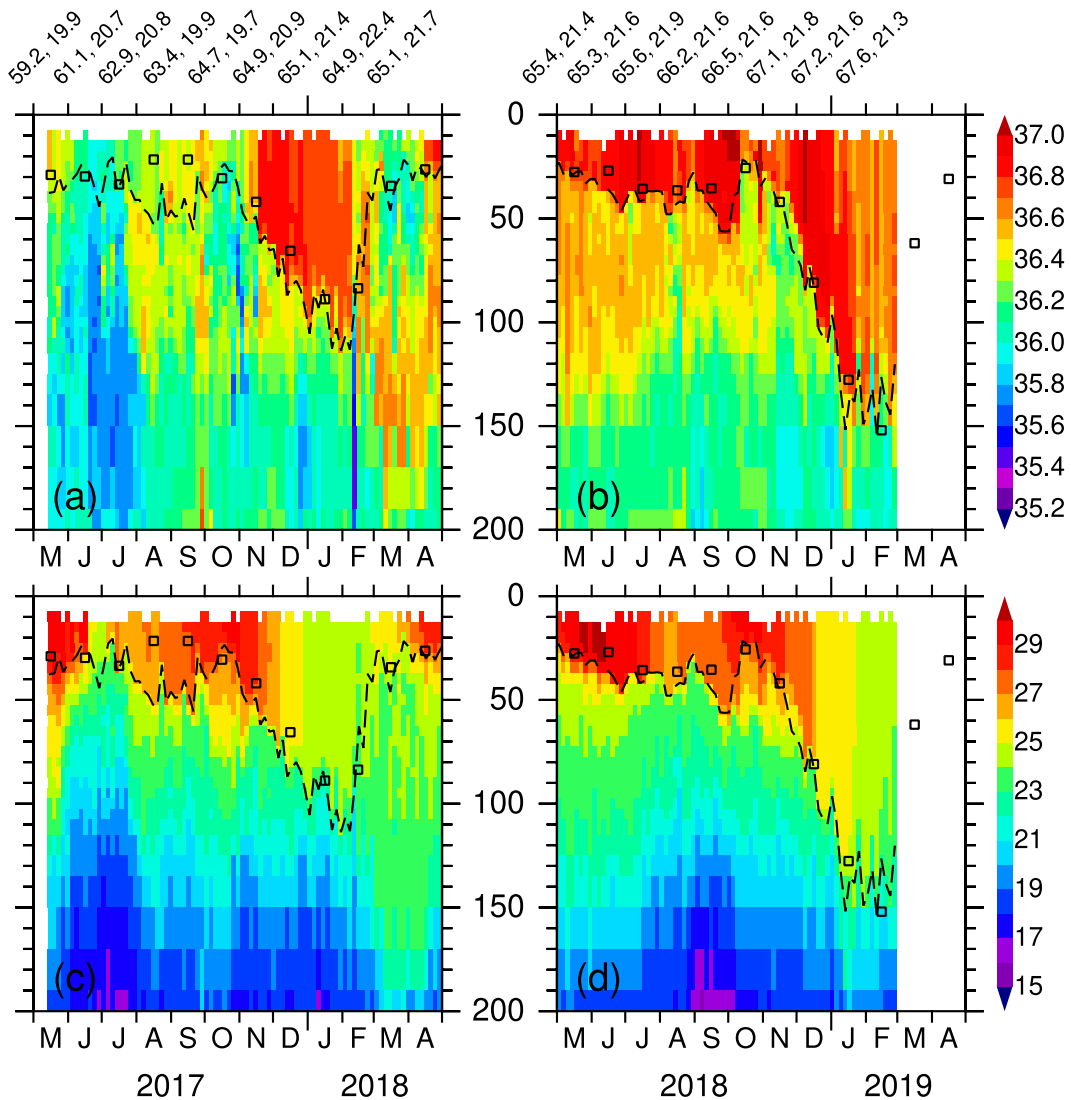


FIG. 1. Evolution of (a),(b) salinity (psu) and (c),(d) temperature ($^{\circ}\text{C}$) measured by an Argo float (ID 2903129) in the northern Arabian Sea during May 2017–February 2019. MLD based on density increase equivalent to a temperature decrease by 1°C is superimposed as dashed lines. Note that the first depth used for MLD calculation is 15 m since no Argo observations are available near the surface. The monthly mean MLD calculated from the EN4 dataset at 22°N , 67°E is shown as open squares. The geographic location of the Argo float observation is shown at the top. The Argo float remained north of 19°N while drifting eastward and ended abruptly at 21.3°N , 67.6°E in February 2019.

salinity with a peak value of 0.20–0.25 psu, thus favored by deep convection. Conversely, 2017–18 salinity anomalies are below the long-term mean and thus indicate suppressed convection. These are consistent with the anomalies in the mixed layer depth with strong (weak) convective mixing generating positive (negative) subsurface salinity anomalies. The mixed layer depth anomalies during 2017/18 and 2018/19 winters are -30 and 40 m, respectively. This further suggests that the salinity anomalies result from the contrasting winter convective mixing and a 1D model is considered to be representative of the physical processes.

The salinity differences depicted in Fig. 2 also show a region of southward-penetrating high salinity (0.1–0.2 psu) at

$\sim 70^{\circ}\text{E}$ in 2019. It is not likely due to the newly formed ASHSW as the winter convection and formation of ASHSW occurs north of $\sim 20^{\circ}\text{N}$ (Prasad and Ikeda 2002a). It appears to be advected southward from the formation region north of 20°N . However, the prevailing WICC flows northward during this period and thus does not favor the advection of high-salinity water from north. This suggests that its origin can be traced back to the previous summer monsoon circulation. The basinwide clockwise circulation during the summer monsoon advects ASHSW southward toward the equator along the eastern part of the Arabian Sea (Prasad and Ikeda 2002b). Furthermore, the WICC flows southward during the summer monsoon, which favors southward advection. Hence, it is

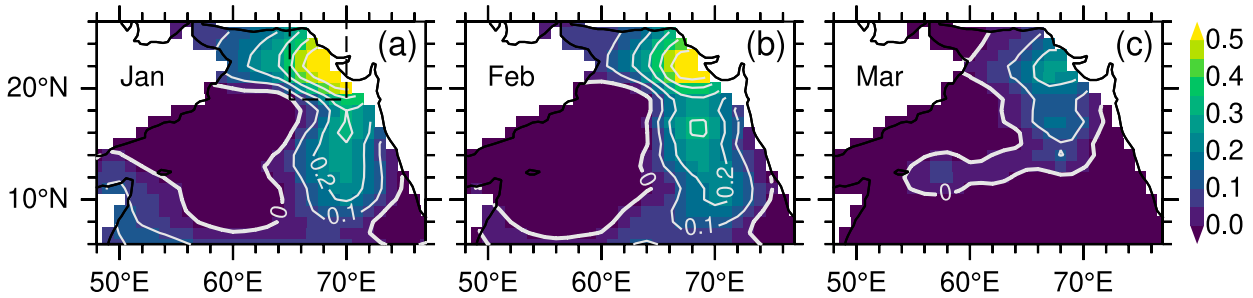


FIG. 2. Monthly mean salinity (psu) differences at 120 m between 2019 and 2018 during (a) January, (b) February, and (c) March from the EN4. Salinity difference in excess of 0.4 psu is observed in the northeast Arabian Sea, which is consistent with the along-track Argo observations. Positive values indicate higher salinity in 2019. The southward extending high salinity at 70°E is the remnants from the summer monsoon.

most likely the remnants from the previous summer monsoon due to changes in the monsoonal circulation. This is further confirmed from comparisons with 1D model results (section 3b), which in the absence of advective processes failed to reproduce the southward high-salinity penetration. Nevertheless, given the agreement between the Argo float observations and EN4 on the existence of high-salinity water north of 20°N, the remainder of the study is focused on the northeastern Arabian Sea north of 20°N.

b. One-dimensional model simulations

The formation of ASHSW can be approximated in a one-dimensional process where loss of surface buoyancy flux is balanced with fluxes at the base of the mixed layer in the absence of horizontal processes (Prasad and Ikeda 2002a,b). HYCOM configured for a mesh of 1D models is applied for the Arabian Sea during the period 2017–18 and 2018–19 separately. Both simulations (2017 and 2018) are initialized in May from the identical GDEM4 climatological temperature and salinity profiles in May. The model is started in May when the wind forcing is weakest and mixed layer is the shallowest owing to surface heat gain by the ocean and integrated over a year using hourly CFSR atmospheric forcing of the respective year 2017–18 and 2018–19. The 1D model is

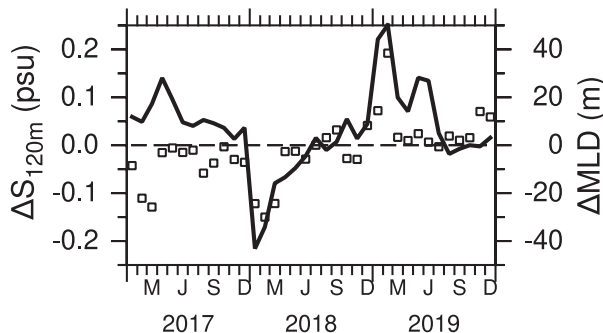


FIG. 3. Area averaged (65°–70°E, 20°–26°N) subsurface salinity anomaly (psu) at 120 m and mixed layer depth anomaly (m) at 22°N, 67°E (open squares) from the EN4 and during the 2017–19 period relative to 2010–19 climatology. These anomalies are consistent with the Argo observations.

evaluated at a location 22°N, 67°E in the northeastern Arabian Sea where significant mixed layer depth differences occurred in the Argo float observations. Figure 4 depicts the evolution of salinity, temperature and mixed layer depth at 22°N, 67°E from the 1D model simulations. The contrasting winter mixed layer simulated by the 1D Model agrees quite well with the along-track float observations and EN4. Specifically, the intensity and duration of the winter convection for both periods are consistent with the observations. For both periods 1D MLD is shallower than the observations by 5–10 m due to error in the surface fluxes and neglect of horizontal processes. The winter mixed layer depth over the period 2018–19 is significantly deeper (143 m) than that in 2017–18 (103 m). This mixed layer depth difference of 40 m is consistent with the observations (Fig. 1). The fact that both simulations are initialized from identical initial conditions in May, differences in the winter mixed layer are due to the differences in the atmospheric forcing. This suggests that buoyancy loss and associated winter cooling during the 2018–19 is stronger than the 2017–18 period. The winter mixed layer depth during 2018–19 is not only deeper but also prolonged into 25 March 2019. On the other hand, the transition from deep winter mixed layer to a shallow spring mixed layer during 2017–18 occurred a month earlier in 26 February 2018. These contrasting mixed layer patterns are also in agreement with the EN4. The long deepening period is followed by an abrupt restratification with a mixed layer depth of 20 m.

The evolution of mixed layer salinity between the two periods shows significant differences (Fig. 4). The mixed layer salinity during the winter 2018–19 is higher than the 2017–18 by 0.2–0.3 psu. The higher salinity during 2018–19 is consistent with the along-track Argo observations (Fig. 1). A noteworthy difference, however, is the occurrence of a significant freshening during the summer of 2017 and associated reduction in salinity (0.7 psu) compared to summer of 2018. Salinity starts decreasing in early July with the arrival of the summer monsoon and reaches a minimum value of 36 psu during August–September 2017. As a consequence, the salinity in the ensuing winter increases only to 36.4–36.5 psu. In the absence of such a freshening in the summer of 2018, the ensuing winter salinity increases to 36.8 psu. Thus, the shallow

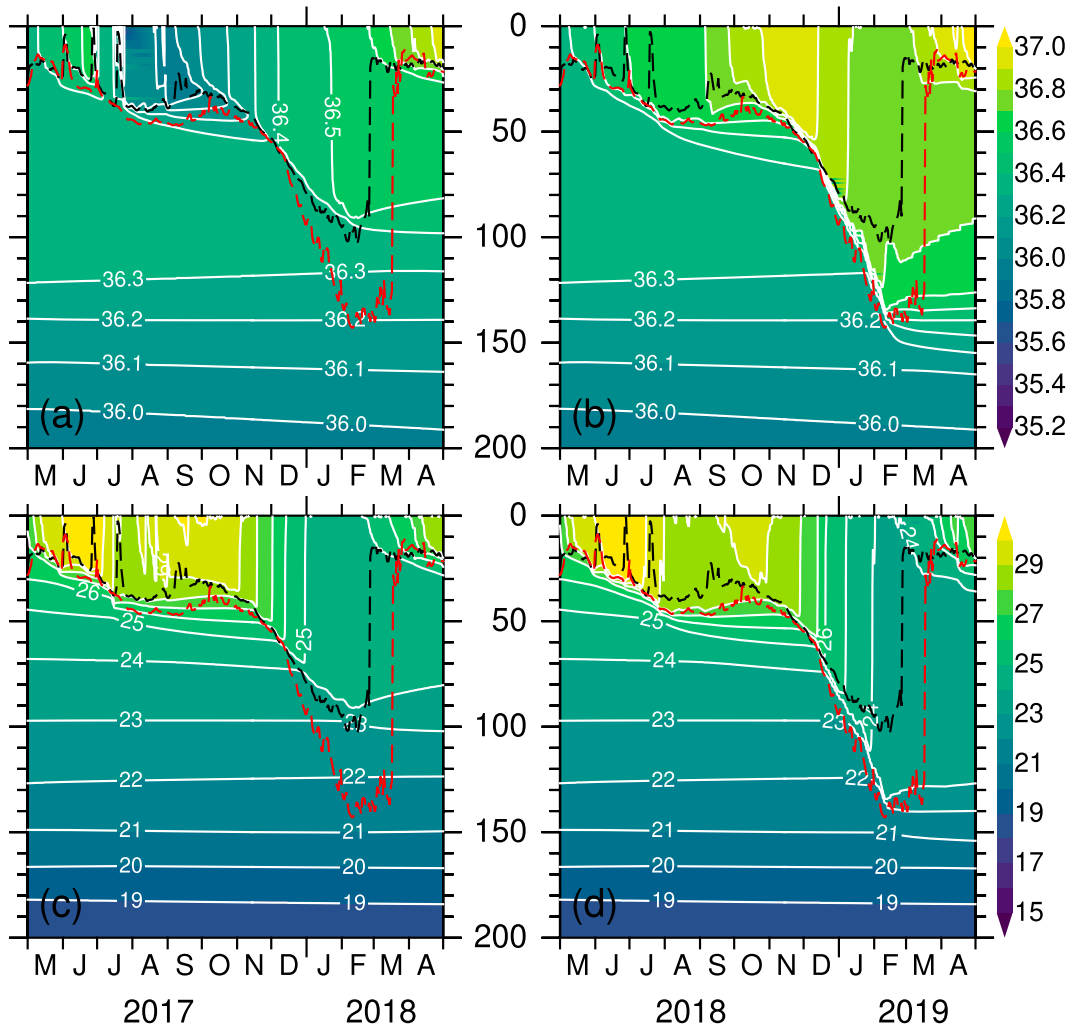


FIG. 4. Time series of 1D model (a),(b) salinity (psu) and (c),(d) temperature ($^{\circ}\text{C}$) at 22°N , 67°E in the northeastern Arabian Sea during 2017–18 and 2018–19 periods. Mixed layer depth based on density increase equivalent to a temperature decrease by 1°C is shown as black (2017–18) and red (2018–19) dashed lines. Both simulations are initialized from identical GDEM4 climatological temperature and salinity profiles for the month of May and integrated forward one year. A year is considered to run from 1 May to the following 30 April. The contrasting mixed layer depths resemble those in the Argo float observations but are shallower during both periods.

(deep) winter mixed layer depth during 2017–18 (2018–19) is preceded by low (high) salinity water and the difference in the stratification may have contributed to the different convective mixing. The evolution of temperature is comparable for the two periods with two exceptions (Figs. 4c,d). Strong stratification during the freshening period (August–September 2017) results in a warmer (1°C) and shallower mixed layer (10 m) and associated warming in the following winter. The fact that both simulations started from identical initial conditions, the higher net precipitation and higher downward net surface heat flux during the first period have contributed to the freshening and warming in the summer of 2017. However, the temperature difference does not explicitly explain the contrasting winter mixed layer depths, indicating that the salinity stratification during the summer that precedes winter

convection also must be considered as a preconditioning of the water column.

Given the agreement between the Argo float observations and the 1D model, we further explore the spatial patterns during winter. This also confirms the dominant role of 1D processes to explain the EN4 salinity difference displayed in Fig. 2 and to evaluate the role of horizontal advection in the formation of ASHSW. Figures 5a–c show salinity differences at 110 m during January–March from the 1D Model. Qualitatively, the evolution of salinity differences in the northeastern Arabian Sea north of $\sim 18^{\circ}\text{N}$ is similar to those in EN4 (Fig. 2). For both periods, the convective mixing during January is similar with a salinity difference of ~ 0.1 psu, which is smaller than that in EN4 (0.5 psu). This discrepancy stems from the fact that 1) 1D model simulations are started from identical

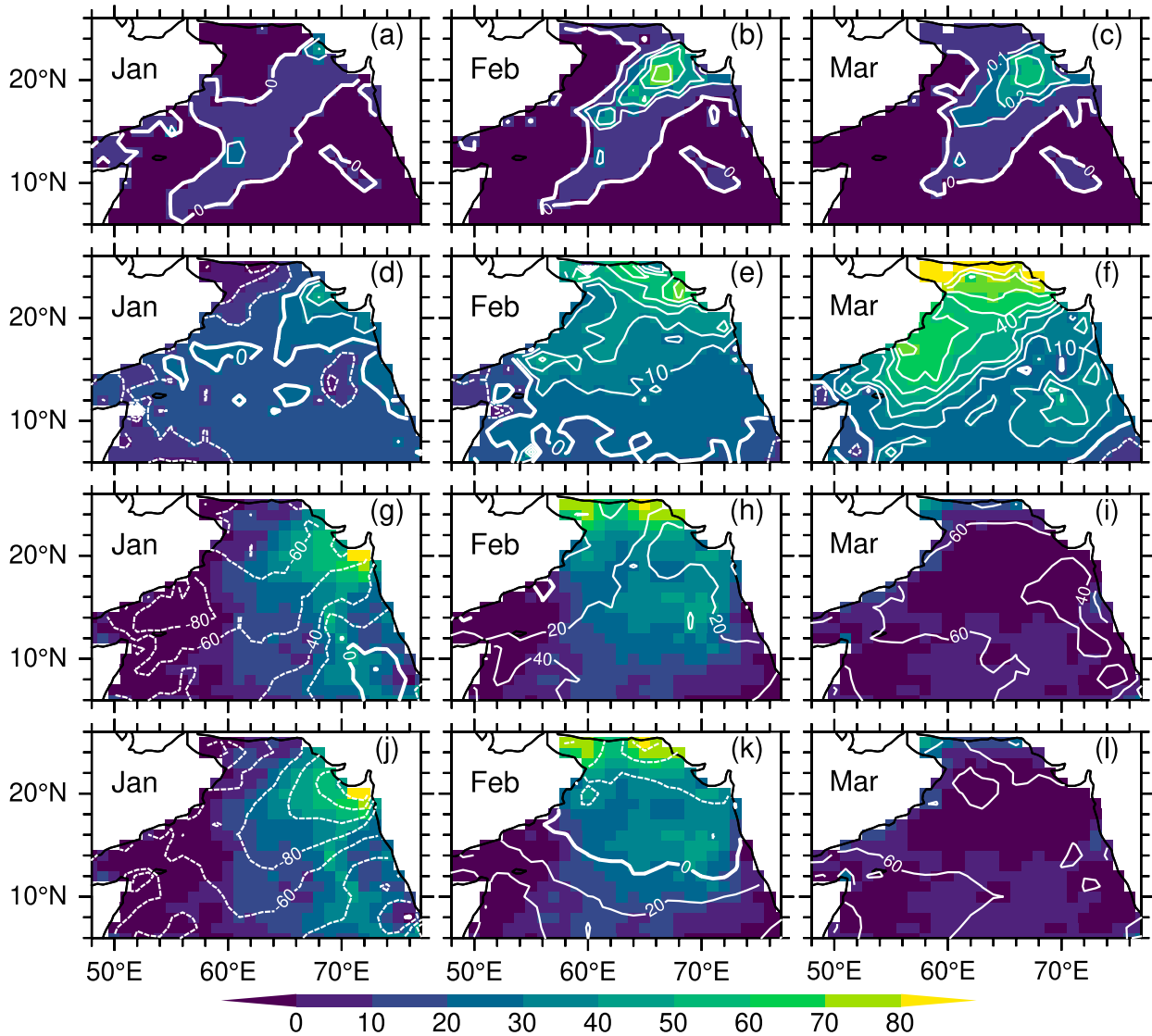


FIG. 5. 1D model monthly mean differences of (a)–(c) salinity at 110 m and (d)–(f) mixed layer depth (m) between 2018 and 2019 during January–March (shaded, contours). Positive values indicate higher salinity in (a)–(c) and a deeper mixed layer in (d)–(f) in 2019 than 2018. Monthly mean surface heat flux (W m^{-2}) during January–March for the year (g)–(i) 2018 and (j)–(l) 2019. Positive (negative) heat flux indicates heat gain (loss) by the ocean. Contour intervals are 0.1 psu in (a)–(c), 10 m in (d)–(f), and 20 W m^{-2} in (g)–(l). Monthly mean surface heat flux differences between 2018 and 2019 are shaded in (g)–(i) and repeated in (j)–(l) with intervals of 10 W m^{-2} as indicated by the color bar at the bottom. The differences are calculated by subtracting the year 2019 from 2018.

initial conditions 2) depth of convective mixing in the EN4 during January 2019 (130 m) is deeper than the 2018 (90 m) by 40 m (Fig. 1). In contrast, the mixed layer difference in the 1D model during January is about 15 m. As the convective mixing during February 2019 becomes deeper, the salinity difference increases to 0.3–0.4 psu. This salinity difference persists into March as the deep convective mixing prolonged into late March 2019 (Fig. 5f). Thus, the enhanced winter convective mixing during 2018–19 results in a 0.2–0.3 psu salinity increase at the base of the mixed layer. The 1D model results can be used to explain the spatial salinity pattern in the EN4. Specifically, the southward penetration of high-salinity water

at 70°E (south of $\sim 18^{\circ}\text{N}$) seen in the EN4 (Fig. 2). The absence of this feature in the 1D model (Figs. 5a–c), which does not account for lateral advection and mixing, further confirms its existence due to the horizontal processes.

The mechanisms of convective mixing and associated salinity changes during the contrasting monsoons are explored using surface heat flux from the 1D model. The surface heat flux for 2018 and 2019 during January–March and their differences are shown in Figs. 5g–l. The heat flux differences between the periods resemble those of the depth of convective mixing (Figs. 5d–f) and salinity. During winter the surface heat loss dominates buoyancy loss in the northern Arabian

Sea while freshwater flux ($E - P$) is expected to play a secondary role. The surface heat loss during 2018–19 is found to be much stronger than 2017–18. Specifically, the northeastern Arabian Sea experiences a surface heat loss in excess of $80\text{--}100\text{ W m}^{-2}$ during January 2019 compared to 60 W m^{-2} heat loss in January 2018. A heat loss of $20\text{--}40\text{ W m}^{-2}$ continued into February 2019 as opposed to a heat gain of $20\text{--}40\text{ W m}^{-2}$ in February 2018 north of 18°N . Assuming a month lag for the mixed layer to respond to the imposed surface heat flux, the prolonged surface heat loss through February 2019 results in a mixed layer deeper than $40\text{--}80\text{ m}$ during March 2019 (Fig. 5f). In contrast, the heat gain by the ocean during February–March 2018 ($20\text{--}60\text{ W m}^{-2}$) leads to an early restratification which results in a shallower mixed layer due to weak mixing under restratified ocean. As a result, the convective mixing in 2018 is short-lived. Both periods show a heat gain by the ocean during March (60 W m^{-2}). Thus, it can be concluded that the surface heat fluxes during the contrasting monsoons contributes to the anomalous convective mixing and salinity differences.

c. 1D model perturbation experiments

To further explore the extent the atmospheric forcing modulated the convective mixing and to identify and isolate the drivers that caused convective mixing differences, we perform five perturbation experiments using the 1D model. This is achieved by replacing each component of the atmospheric forcing with a different period. We used the 2018–19 as a baseline run and subsequently replaced each components of the forcing from the 2017–18 period. The results are summarized in Fig. 6. As a reference, mixed layer depth from the control experiments (unperturbed) for the periods 2017–18 and 2018–19 are shown. In the northern Arabian Sea, drier and cooler air is known to be the dominant factor affecting winter heat loss (Prasad and Ikeda 2002a). To isolate the effect of specific humidity, we performed an experiment (referred as SH) by replacing 2018–19 with 2017–18 specific humidity while other forcing is retained. Except during February–March, the evolution of mixed layer depth is identical to the 2018–19 control run. Specifically, the mixed layer transition from winter to spring occurred a month earlier, consistent with the 2017–18 control run. The specific humidity difference also results in a shallower mixed layer in February by $5\text{--}10\text{ m}$. The response of SST to the specific humidity is to increase the winter SST up to 1.2°C to be consistent with the 2017–18 control run (Figs. 6b,c). This implies that drier and colder air emanated from the north by northeast monsoon during the 2018–19 winter enhanced the latent heat flux resulting in an excess heat loss. Thus, it can be concluded that the winter convective mixing that extended into late March 2019 is due to the specific humidity differences.

The second experiment is designed to examine the response of the winter mixed layer to the excess freshwater flux (precipitation > evaporation) in the preceding summer monsoon as is the case during 2017–18 (Fig. 4a). In the precipitation perturbation experiment (PP), the 2017–18 precipitation is imposed while other 2018–19 forcing is retained. The excess

precipitation has a larger impact on the depth of winter convective mixing. The winter mixed layer is shallower than the 2018–19 control run by 23 m preceded by precipitation induced salinity stratification during the summer. This accounted for 50% of the winter mixed layer depth difference between the contrasting periods. In contrast, the summer mixed layer is shallower by 5 m , indicating its larger impact on the ensuing winter mixed layer depth. The mixed layer depths between the PP and 2017–18 control runs remain similar until early February, indicating that mixed layer depth is governed by similar atmospheric forcing. The rate of winter mixed layer deepening is less abrupt in the PP compared to 2018–19 during December–January. The response of SST to the excess precipitation is negligibly small (Figs. 6b,c). This experiment suggests that the precipitation induced salinity changes during the summer favored a strong stratification, preconditioning for a slow and weak winter convective mixing.

Although preceding perturbation experiments are performed to isolate the role of each forcing component, we now examine the combined effect of various forcings due to the fact that changes in specific humidity are accompanied by changes in air temperature and precipitation. The combined effect of specific humidity and precipitation is diagnosed in an experiment (PPSH) in which both forcings are prescribed to use 2017–18 while other forcing is retained. This results in a shallower winter mixed layer that does compare closely with the 2017–18 control run. The winter mixed layer shoaled from 123 to 92 m and a slightly shallower ($5\text{--}10\text{ m}$) summer mixed layer. The evolution of SST (Fig. 6b) is similar to those in SH due to its response to surface heat flux through latent heat. The precipitation induced freshening decreases salinity by $0.7\text{--}0.8\text{ psu}$ during the summer of 2017 and $0.2\text{--}0.4\text{ psu}$ in the following winter (Fig. 6d). The salinity freshening generates a strong stratification which in turn increased the stability of the water column in the ensuing winter. This results in a shallower convective mixing and associated reduction of salinity at 100 m ($0.3\text{--}0.4\text{ psu}$). The salinity difference between the 2018–19 control run and PPSH (Fig. 6d) is similar to those between the 2017–18 and 2018–19 (Fig. 6e). This further confirms that the salinity difference between the periods 2017–18 and 2018–19 is almost entirely driven by differences in precipitation and specific humidity. The inclusion of air temperature in an experiment (ATPPSH) results in a similar mixed layer depth and SST to those in PPSH. This stems from the small contribution of sensible heat flux due to air–sea temperature differences to the total heat flux. Thus, combined effect of summer precipitation and winter specific humidity yield a significant shallower and short-lived mixed layer during the winter of 2017–18.

Throughout a year, excess evaporation over precipitation dominates the freshwater flux in the northern Arabian Sea and favors the ASHSW formation in winter. In a typical year, this region receives very little or no precipitation during the summer monsoon while the southeastern Arabian Sea and continental India receive a large portion of precipitation (Ramesh Kumar and Prasad 1997; Prasad 1997). Thus, it is highly unlikely that the precipitation in a typical year

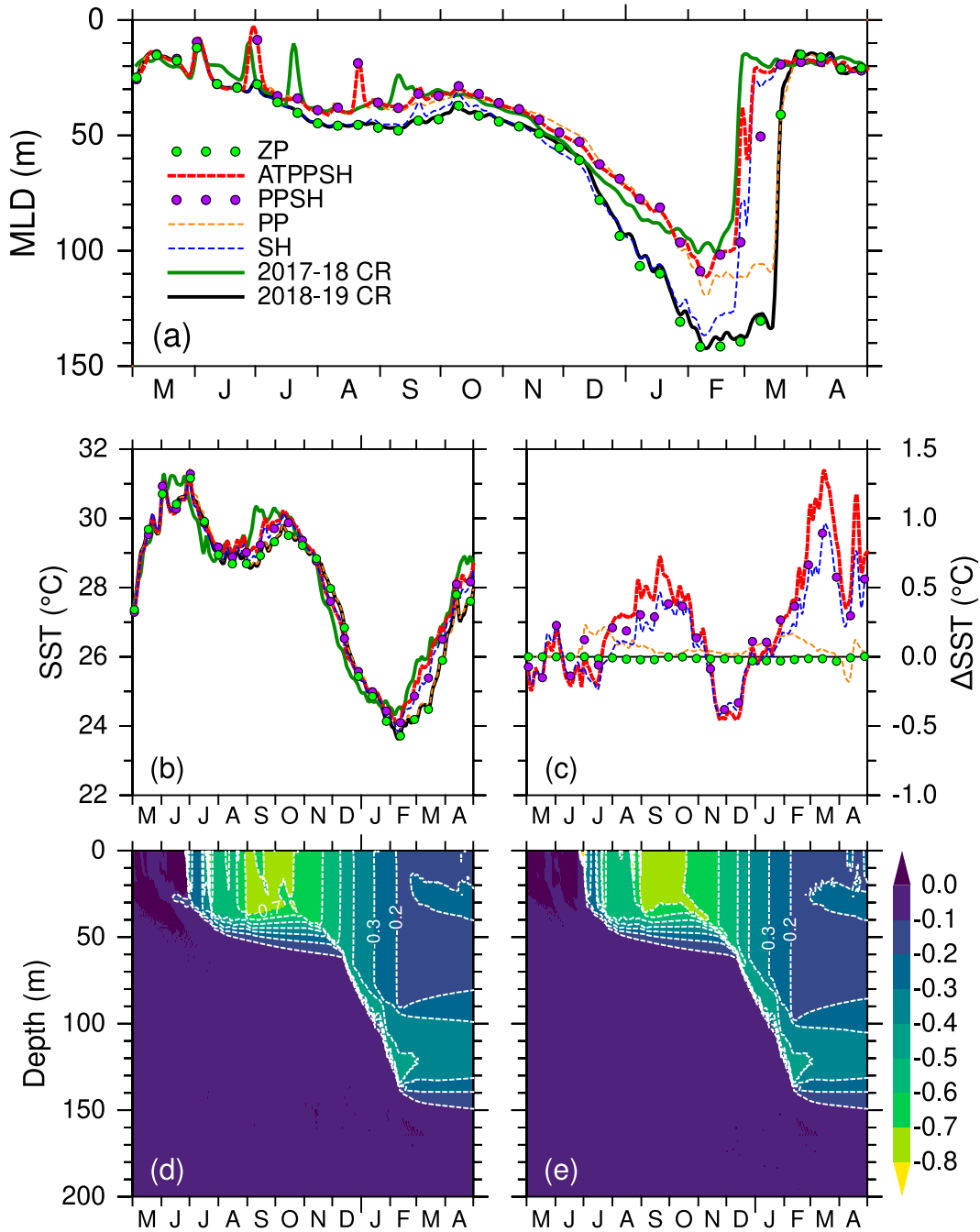


FIG. 6. (a) Mixed layer depth (MLD; m) and (b) SST ($^{\circ}\text{C}$) from control simulations 2017–18 (solid dark green line) and 2018–19 (solid black line), perturbation experiments in dashed lines from SH (blue), PP (orange), PPSH (purple filled circles), ATPSSH (red), and ZP (light green filled circles) at 22°N , 67°E . (c) SST differences between the control simulation 2018–19 and perturbation experiments. The symbols are plotted every 10 (15) days for MLD (SST and SST differences). To distinguish each line, a 5-day Parzen smoothing is applied for MLD, SST, and SST differences. Monthly mean salinity differences from 1D model between (d) the 2017–18 and 2018–19 control runs and (e) the 2018–19 control run and PPSH. All perturbation experiments are started from 2018–19 control simulations by replacing each component of the atmospheric forcing with 2017–18 specific humidity (SH), precipitation (PP), combined specific humidity and precipitation (PPSH), and air temperature (ATPPSH), and zero precipitation in 2018–19 (ZP).

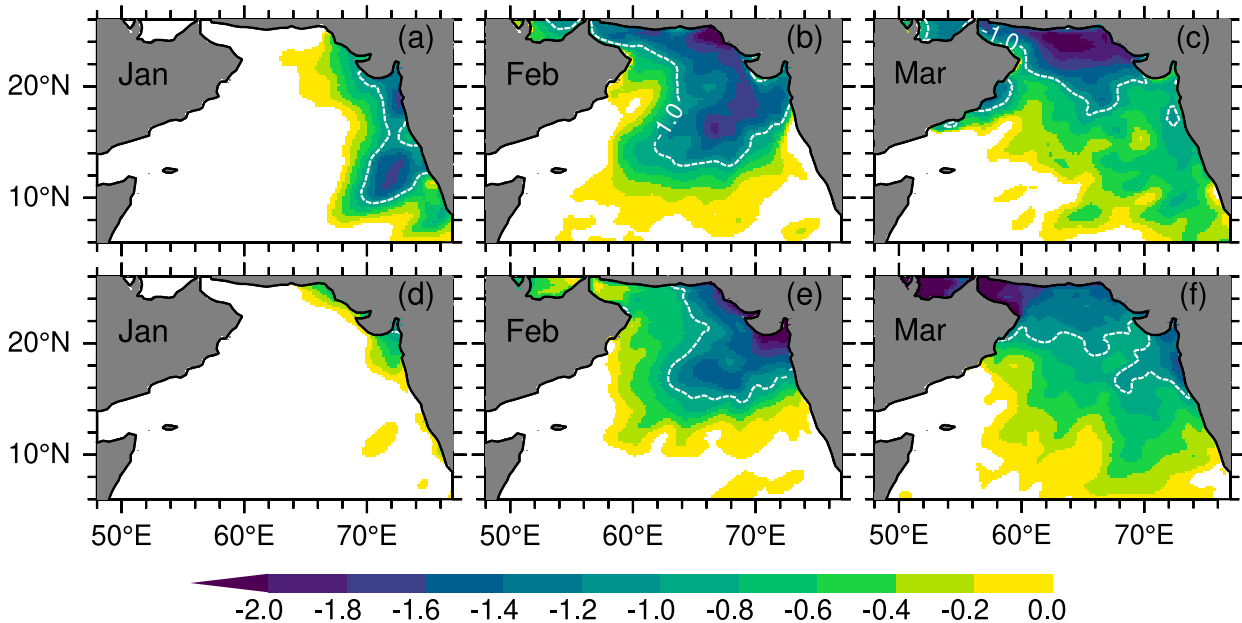


FIG. 7. Monthly mean differences of CFSR forcing (a)–(c) specific humidity (g kg^{-1}) and (d)–(f) air temperature ($^{\circ}\text{C}$) for January–March between 2019 and 2018 (2019 minus 2018). Negative values indicate drier and colder air in 2019 than 2018.

modulates the evolution of salinity and stratification in the northern Arabian Sea. To address this hypothesis, we prescribed a zero precipitation while other forcing is retained (2018–19) in another experiment (ZP). The depth of convective mixing (and SST) in the ZP is identical to those in the 2018–19 control run (Figs. 6a,b). This suggests that the precipitation played no role in the evolution of salinity and 2018–19 can be considered a precipitation deficient year. Thus, winter buoyancy loss preconditioned with a weakly stratified ocean is conducive to deep convective mixing. Our results indicate that the winter convective mixing in the northeastern Arabian Sea exhibits a fundamentally different pattern, depending on the preconditioning of the ocean.

d. Atmospheric forcing

Having identified and isolated the relative role of various factors affecting convective mixing in the 1D model experiments, the atmospheric forcing that contributes to different convective mixing is examined. In Fig. 7 we contrast CFSR specific humidity and air temperature between 2017–18 and 2018–19 periods. During winter, the latent heat loss dominates the buoyancy loss and to a lesser extent by sensible heat flux. Factors affecting latent heat flux include wind speed, surface temperature, and humidity. Strong winds, higher temperatures, and lower specific humidity act to increase latent heat flux, whereas higher humidity tends to decrease latent heat flux. Both specific humidity and air temperature during the winter of 2018–19 are lower than that of 2017–18, indicating prevalence of drier and colder air. The drier air first reaches the northeastern Arabian Sea in December–January and intensifies in February–March with specific humidity differing by $1\text{--}2 \text{ g kg}^{-1}$. Associated with the drier air is the anomalous

colder air temperature ($1^{\circ}\text{--}2^{\circ}\text{C}$) carried by the prevailing northeasterly winds. The combined effect increases the surface heat loss (Fig. 5) from the ocean due to enhanced latent heat flux. The sensible heat flux, which is a function of winds and air–sea temperature difference, is negligibly small and not a major contributor to the surface heat flux.

In addition to contrasting heat flux during winter, it is clear from Fig. 4 that a shallow winter convective mixing in 2017–18 was preceded by an anomalously freshwater flux during the summer of 2017. To elucidate this further, Figs. 8d–f shows freshwater flux (precipitation – evaporation; $P - E$) difference between 2017 and 2018 from the 1D model during June–August. The precipitation dominates the freshwater flux during June–August 2017. Specifically, the northeastern Arabian Sea receives precipitation in excess of 5 mm day^{-1} during this period. Precipitation in August is still high but slightly declined from July. The sustained precipitation generates anomalously low-salinity water ($>0.5 \text{ psu}$) during the 2017 summer monsoon (Fig. 8a) and its maintenance into late summer. The low-salinity water increases the stratification which in turn preconditioned the water column during the ensuing winter convection. The seasonal mean (July–September) surface salinity differences between 2017 and 2018 summer from the 1D model, GOFS and EN4 show similar salinity reduction in excess of 0.2 psu in the northeastern Arabian Sea, although the spatial extent of the freshening differs in these products (Figs. 8a–c). In addition to vertical mixing due to turbulent diffusion and local convection, GOFS includes horizontal advection and vertical advection due to horizontal convergence and divergence and lateral turbulent mixing that is missing in a 1D model. Differences in salinity between the 1D and GOFS can be attributed to these processes. In GOFS the

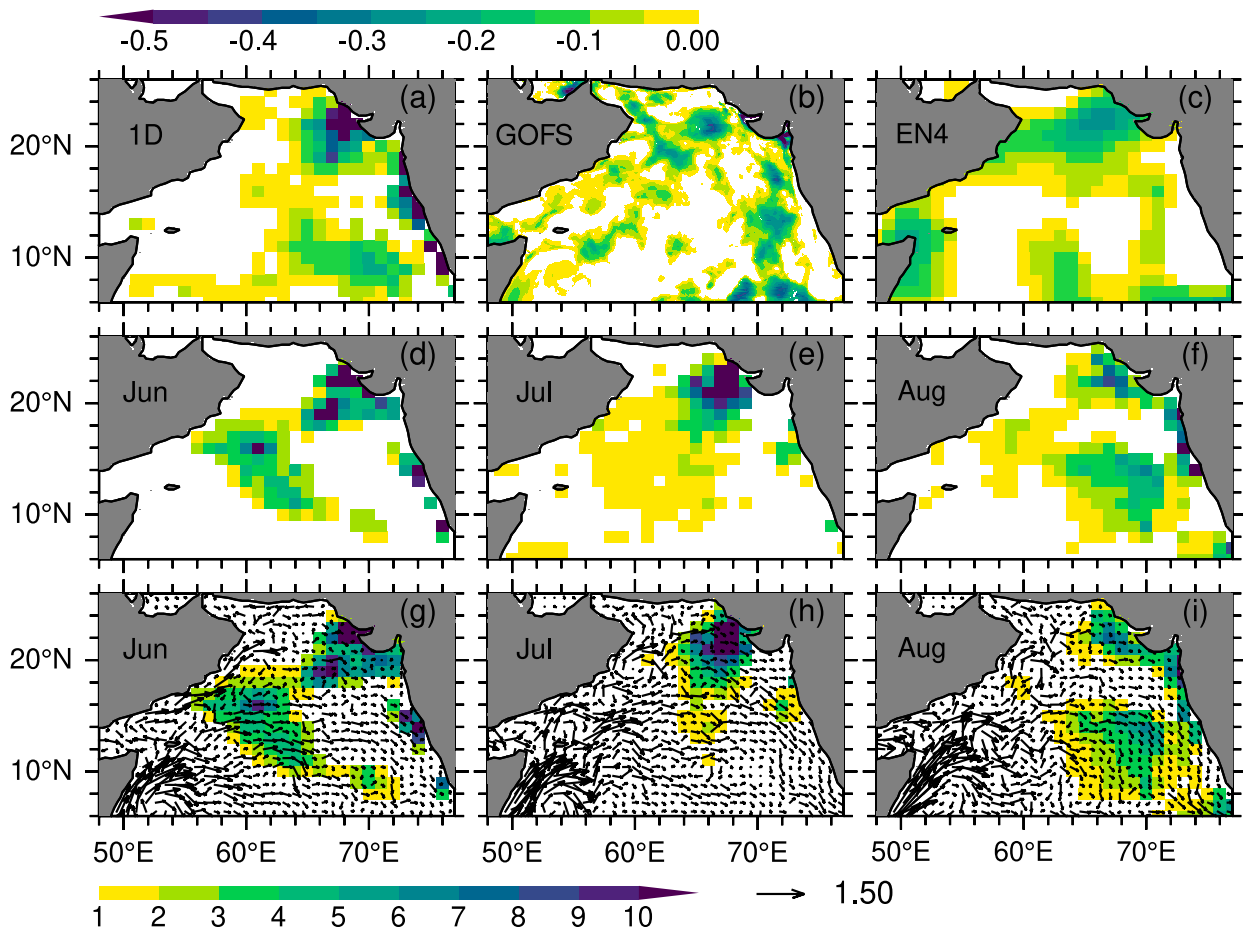


FIG. 8. Seasonal mean (July–September) surface salinity differences between 2017 and 2018 summer from (a) 1D model, (b) GOFS, and (c) EN4. Negative values indicate salinity decrease in 2017 relative to 2018. (d)–(f) 1D model monthly mean freshwater flux (precipitation – evaporation; mm day^{-1}) difference between 2017 and 2018 during June–August. Positive values indicate excess precipitation over evaporation during the summer 2017. (g)–(i) GOFS monthly mean surface currents (m s^{-1}) during June–August 2017 overlaid on CFSR monthly mean precipitation difference (mm day^{-1}) between 2017 and 2018 with positive values indicating excess precipitation in 2017.

freshening is confined to a smaller area around 22°N , 66°E , which may have been influenced by mesoscale eddies. The fact that the salinity pattern is qualitatively similar between the 1D and GOFS models suggest that 1D processes dominated the maintenance of low salinity. On the other hand, despite large freshening the freshwater induced salinity reduction in the 1D model is qualitatively comparable with the EN4. It is worth mentioning that precipitation forcing for the GOFS and 1D model came from the NAVGEM and CFSR, respectively.

The precipitation induced salinity changes and its maintenance into late summer suggest that ocean dynamical processes acted in favor of sustaining the freshening. Strong winds and ocean currents induce wind-driven mixing and advection that act together to dampen the freshwater induced salinity changes. During summer monsoon, the wind-driven mixing in the northeastern Arabian Sea is significantly weaker than the regions surrounding Somalia, where the wind-driven mixing is strongest due to the Findlater Jet. Under low-wind

conditions, the wind-driven mixing is unable to break the freshwater induced stratification, resulting in a shallow mixed layer depth of ~ 25 m in the northeastern Arabian Sea (Fig. 4). This leads to the maintenance of stratification and low-salinity water into the ensuing winter monsoon.

Ocean advection can dampen the freshwater induced salinity changes and modulate the stratification. This is examined qualitatively using surface currents from the GOFS during June–August 2017 (Figs. 8g–i). Surface currents in the northeastern Arabian Sea are significantly weaker than in the western Arabian Sea, where the Findlater Jet drives strong currents along the coasts of Somalia, Saudi Arabia and Oman and associated mesoscale eddies resulting from baroclinic instabilities. In the northeastern Arabian Sea, the surface velocity fluctuates between eastward and southeastward with preferred southeastward direction. The current speed varies from 10 to 20 cm s^{-1} . These weak currents failed to dampen the freshwater anomalies, thereby contributing to the maintenance of low-salinity water. While precipitation influences

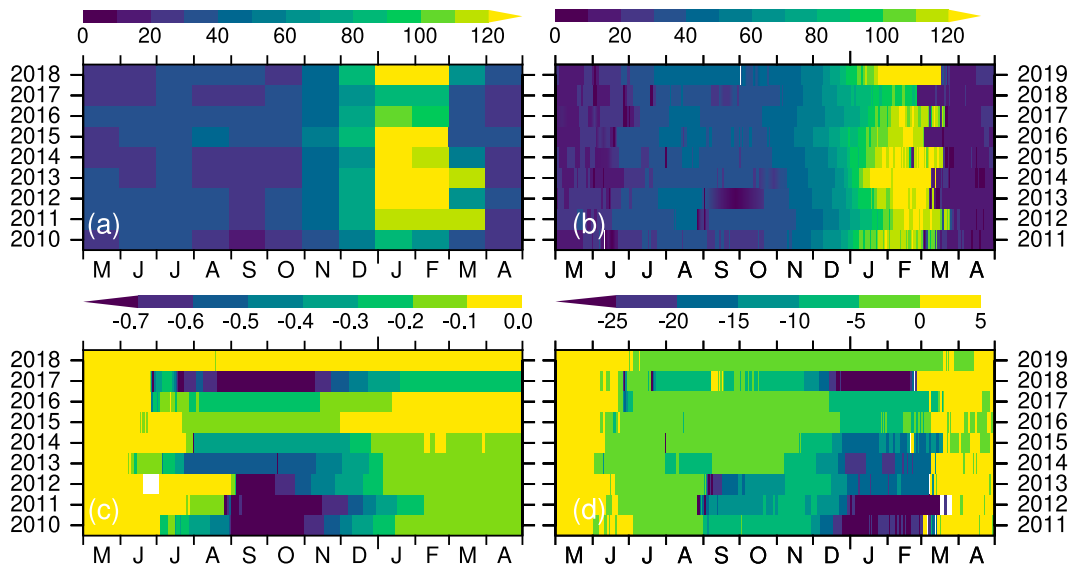


FIG. 9. Temporal evolution of mixed layer depth (m) from (a) EN4 and (b) 1D model, and differences in 1D model (c) sea surface salinity (psu) and (d) mixed layer depth between the 1D experiments ZP and control runs for years from 2010 to 2011 to 2018–19. Negative values indicate lower salinity in (c) and shallower MLD in (d) in the ZP experiment. All simulations started from same initial conditions in May of each year and integrated for one year. Note that y axis is years, and 2010 refers to the 2010–11 period, spanning from May 2010 through April 2011.

salinity at various scales, salinity is expected to be quickly restored after a short-lived precipitation event. However, the seasonal accumulation of precipitation during the summer monsoon 2017 far exceeds such short-lived events and hence contributed to maintaining the salinity stratification.

e. Interannual context

The winter mixed layer response to contrasting atmospheric forcing raises a question: was the 2017 summer an anomalous year of precipitation? The interannual context of winter convective mixing observed during winter 2017–19 is further investigated with a special focus on the freshwater flux that preceded the winter. We performed two 1D model simulations at 22°N, 67°E for the period spanning from 2010 to 2018. Each 1D simulation is reinitialized in May from GDEM4 temperature and salinity and integrated for a year. In addition to the control simulations (ICTL), we performed 1D model perturbation experiments in which zero precipitation (IZP) is imposed while other forcing is retained. A comparison of mixed layer depth between the EN4 and 1D model (Figs. 9a,b) reveals a qualitative agreement on the depth of winter convective mixing with large year-to-year variability. Of particular interest is the duration of winter convective mixing modulated by buoyancy forcing. The termination of winter convection, characterized by the beginning of restratification, is evident from the nine winters and vary between early to late March. The winters extending into late March include 2011–12, 2014–15, 2016–17, and 2018–19 while the early termination winters include 2012–13, 2015–16, and 2017–18. These changes in the duration of winter convection can significantly alter the ASHSW formation in addition to the depth of convection as is evident from 2017 to 2019

contrasting periods. It should be noted that the transition from a deep winter to a shallow spring mixed layer occurs more rapidly in the 1D model while those in the monthly mean EN4 show a gradual transition. This is because the 1D model in the absence of lateral mixing responds quickly to the heat gain by the ocean. The winter mixed layer in the 1D model is consistently shallower than the observations, possibly due to errors in the atmosphere fluxes.

To isolate the effect of precipitation on the salinity stratification and associated mixed layer response, Figs. 9c and 9d depict sea surface salinity and mixed layer depth differences between the ICTL and IZP. It is evident from the nine winters that the period 2017–18 stands out as by far the shallowest winter mixed depth (shallower by 25 m) and the largest summer freshening (0.7 psu). Moderate to strong freshening is also evident over the period 2010–11 to 2013–14 although the duration and timing of summer freshening vary. The freshening during September–November 2017 occurs after the peak months of summer monsoon (June–August). Regardless of timing, the impact of summer freshening on the ensuing winter convective mixing is clear as evidenced by the shallower winter mixed layer depth (15–20 m). Weak precipitation induced salinity changes (0.1–0.3 psu) over the period 2015–18 (with the exception of 2017) result in a weak winter mixed layer response (~10 m). The salinity anomaly (0.1 psu) and mixed layer (5 m) responses to precipitation are minimal during 2018–19 due to below average precipitation. These results suggest the summer freshening in 2017 is strong but not exceptional, causing an anomalously shallow mixed layer in the ensuing winter of 2017–18. Conversely, the precipitation deficient summer of 2018–19 is exceptional resulting in an anomalously deep winter

mixed layer. Thus, the summer precipitation preconditions the water column as it increases the stratification and suppress the ensuing winter convection.

4. Discussion and conclusions

The formation and spreading of Arabian Sea High Salinity Water (ASHSW) in the northern Arabian Sea plays an important role in the salt-budget of the Indian Ocean. The advection of relatively low-salinity water from the Bay of Bengal by the East India Coastal Current (EICC) and Northeast Monsoon Current mixes with the high-salinity water in the Arabian Sea. This low-salinity water is carried northward along the coast of India by the West Indian Coastal Current (WICC). During summer monsoon, the basinwide clockwise circulation advects high-salinity ASHSW toward the equator along the eastern part of the Arabian Sea, which is subsequently carried into the Bay of Bengal by the eastward flowing Indian Monsoon Current (IMC). Although winter convective formation of ASHSW is an annual event in the northern Arabian Sea, our results indicate that it presents a high degree of interannual modulation concerning its duration and spatial extent due to interannual variability of the winter atmospheric conditions. Specifically, the persistent cold and dry air (low specific humidity) from the northeast by prevailing northeasterly winds contribute to prolonged winter convective mixing.

Although winter convective mixing is a response to the local surface buoyancy loss from the ocean, mainly due to the heat loss, we show the modulation of winter convective mixing resulting from the freshwater induced salinity stratification from the summer conditions preceding winter. This presents another important source of interannual variability, which has not been considered a source before, in the convective formation of ASHSW. In the northern Arabian Sea, the interannual variability of precipitation is largely associated with the strength of summer monsoons and the availability of moisture, which is carried by the southwesterly winds. Persistent low pressure systems usually form in the Bay of Bengal, and their interaction with other local systems (e.g., synoptic scale, mesoscale, large scale) can lead to extreme precipitation during the summer monsoon. In 2017, the existence of two low pressure systems that stretched over northern Bay of Bengal to northwestern India, brought one of the worst catastrophic floods in the states of Gujrat and Rajasthan in terms of both rainfall amount and the number of people affected (Roxy et al. 2017; Kumar et al. 2020). These low pressure systems interacting with moist winds from the west (western disturbances) lead to extreme precipitation over the northeastern Arabian Sea. The mixed layer response to summer precipitation was highly unusual that it affected the ensuing winter by inhibiting the convective mixing to a shallow depth.

The major conclusions drawn here are based on 1D model experiments. The winter convective mixing in the northern Arabian Sea is governed by surface buoyancy loss and can be represented reasonably well in a 1D model (Prasad and Ikeda 2002a). Thus, the assumption is not untenable to the process under study. Unlike the northwestern Arabian Sea, where

advection of high-salinity water from the Gulf of Oman by mesoscale eddies is likely modulate the ASHSW (Zhang et al. 2020), the northeastern Arabian Sea by comparison is less prone to mesoscale eddies. The northward advection of low-salinity water from the Bay of Bengal by WICC is limited to south of 20°N and hence does not modulate the water-mass formation processes. The horizontal advection and mixing, which 1D model does not include, play an important role in the seasonal spreading of the ASHSW (Prasad and Ikeda 2002b; Zhang et al. 2020). Specifically, the northward currents along the coasts of Saudi Arabia and Oman, coastal upwelling, Ras Al Hadd Jet (Schott and McCreary 2001), and mesoscale eddies (Flagg and Kim 1998), all significantly affect the ASHSW during the summer monsoon. Furthermore, the mesoscale eddies near the mouth of the Gulf of Oman carries ASHSW into the northern Arabian Sea (L'Hégaret et al. 2013; Wang et al. 2013; Zhang et al. 2020) generating anomalous salinity events. Perhaps the most important role of ocean advection during the summer monsoon is to dampen the freshwater induced salinity changes triggered by excess precipitation. We find that this contribution was not dominant in 2017 owing to extreme precipitation that persisted over several months in a region with relatively weak currents and mesoscale eddy activity. However, when precipitation influences salinity at shorter time scales (days to a week), advection can dampen the freshwater induced salinity changes and quickly restore the salinity to its magnitude before the precipitation event.

In spite of these caveats, the 1D model used in this study includes mechanisms controlling the winter mixed layer in the northeastern Arabian Sea. It simulates to a reasonable extent the amplitude and the year-to-year observed winter mixed layer variability. We find that the period 2017–19 stood out by as far as the having deepest winter mixed layer depths in the northeastern Arabian Sea in the last decade. Our 1D model experiments show that the response of winter mixed layer to atmospheric forcing is not only influenced by local surface buoyancy loss (amplified by specific humidity) but also a preconditioned response to freshwater fluxes and associated buoyancy gain by the ocean during summer preceding the winter. During the 2017–18, the excess precipitation over evaporation during the summer monsoon precedes a shallower and short-lived winter mixed layer. The freshwater induced salinity stratification (−0.7 psu) during the summer inhibited the convective mixing in the ensuing winter, resulting in a shallower winter mixed layer (103 m). This combined with weak buoyancy loss due to weaker than usual latent heat loss, explained by higher than usual specific humidity in the northeastern Arabian Sea, caused an early termination of the convective mixing (26 February 2018).

In contrast, during the 2018–19 the winter convective mixing was deeper and long-lived. The 2018 summer by comparison was characterized by normal or below precipitation and generated a weaker stratification preconditioned to winter mixing. As a result, convective mixing is more intense and deeper by mixing cooler and saltier waters down to 143 m. This combined with colder and drier from air from the north and its lower specific humidity produced larger latent cooling

and buoyancy loss in the northeastern Arabian Sea. This resulted in a prolonged winter convective mixing through 25 March 2019. This study underscores the importance of stratification that has preconditioning impact on the winter convective mixing and water mass formation in the northeastern Arabian Sea. The role of this mechanism and process deserve further study.

Acknowledgments. This work was supported by the U.S. Office of Naval Research through the NRL project winter convection (PE 61153N). Computer time was provided by the Department of Defense (DoD) High Performance Computing Modernization Program and the simulations were performed on the Cray XC40 and HPE SGI 8600 supercomputers at the Navy DoD Supercomputing Resources Center, Stennis Space Center, Mississippi.

Data availability statement. The Met Office Hadley Centre series of datasets (EN4) of global quality-controlled ocean temperature and salinity profiles used in this study are openly available at locations cited in Good et al. (2013). Argo float observations are publicly available at argo.ucsd.edu. The NCEP CFSR data are openly available and can be obtained from rda.ucar.edu. HYCOM reanalysis product used in this study can be accessed from www.hycom.org. The 1D model output is available upon reasonable request to corresponding author.

REFERENCES

- Bauer, S., G. L. Hitchcock, and D. B. Olson, 1991: Influence of monsoonally-forced Ekman dynamics upon surface layer depth and plankton biomass distribution in the Arabian Sea. *Deep-Sea Res.*, **38A**, 531–553, [https://doi.org/10.1016/0198-0149\(91\)90062-K](https://doi.org/10.1016/0198-0149(91)90062-K).
- Bleck, R., 2002: An oceanic general circulation model framed in hybrid isopycnic-Cartesian coordinates. *Ocean Modell.*, **4**, 55–88, [https://doi.org/10.1016/S1463-5003\(01\)00012-9](https://doi.org/10.1016/S1463-5003(01)00012-9).
- Böhm, E., J. M. Morrison, V. Manghnani, H. S. Kim, and C. Flagg, 1999: The Ras al Hadd Jet: Remotely sensed and acoustic Doppler current profiler observations in 1994–1995. *Deep-Sea Res. II*, **46**, 1531–1549, [https://doi.org/10.1016/S0967-0645\(99\)00034-X](https://doi.org/10.1016/S0967-0645(99)00034-X).
- Boyer, T. P., and Coauthors, 2009: World Ocean Database 2009. S. Levitus, Ed., NOAA Atlas NESDIS 66, 216 pp.
- Carnes, M. R., R. W. Helber, C. N. Barron, and J. M. Dastugue, 2010: Validation test report for GDEM4. NRL Tech. Rep. NRL/MR/7330-10-9271, 66 pp.
- Chowdary, J. S., and C. Gnanaseelan, 2005: Water mass properties and transports in the Arabian Sea from Argo observations. *J. Atmos. Ocean Sci.*, **10**, 235–260, <https://doi.org/10.1080/17417530600752825>.
- Findlater, J., 1969: Interhemispheric transport of air in the lower troposphere over the western Indian Ocean. *Quart. J. Roy. Meteor. Soc.*, **95**, 400–403, <https://doi.org/10.1002/qj.49709540412>.
- Fischer, A. S., R. A. Weller, D. L. Rudnick, C. C. Eriksen, C. M. Lee, K. H. Brink, C. A. Fox, and R. R. Leben, 2002: Mesoscale eddies, coastal upwelling, and the upper-ocean heat budget in the Arabian Sea. *Deep-Sea Res. II*, **49**, 2231–2264, [https://doi.org/10.1016/S0967-0645\(02\)00036-X](https://doi.org/10.1016/S0967-0645(02)00036-X).
- Flagg, C. N., and H.-S. Kim, 1998: Upper ocean currents in the northern Arabian Sea from shipboard ADCP measurements collected during the 1994–1996 U.S. JGOFS and ONR programs. *Deep-Sea Res. II*, **45**, 1917–1959, [https://doi.org/10.1016/S0967-0645\(98\)00059-9](https://doi.org/10.1016/S0967-0645(98)00059-9).
- Good, S. A., M. J. Martin, and N. A. Rayner, 2013: EN4: Quality controlled ocean temperature and salinity profiles and monthly objective analyses with uncertainty estimates. *J. Geophys. Res. Oceans*, **118**, 6704–6716, <https://doi.org/10.1002/2013JC009067>.
- Han, W. Q., J. P. McCreary, and K. E. Kohler, 2001: Influence of precipitation minus evaporation and Bay of Bengal rivers on dynamics, thermodynamics, and mixed layer physics in the upper Indian Ocean. *J. Geophys. Res.*, **106**, 6895–6916, <https://doi.org/10.1029/2000JC000403>.
- Jensen, T. G., 2001: Arabian Sea and Bay of Bengal exchange of salt and tracers in an ocean model. *Geophys. Res. Lett.*, **28**, 3967–3970, <https://doi.org/10.1029/2001GL013422>.
- , 2003: Cross-equatorial pathways of salt and tracers from the northern Indian Ocean: Modelling results. *Deep-Sea Res. II*, **50**, 2111–2127, [https://doi.org/10.1016/S0967-0645\(03\)00048-1](https://doi.org/10.1016/S0967-0645(03)00048-1).
- Joseph, S., and H. J. Freeland, 2005: Salinity variability in the Arabian Sea. *Geophys. Res. Lett.*, **32**, L09607, <https://doi.org/10.1029/2005GL022972>.
- Kumar, S. P., and T. G. Prasad, 1996: Winter cooling in the northern Arabian Sea. *Curr. Sci.*, **71**, 834–841.
- , and —, 1999: Formation and spreading of Arabian Sea high-salinity water mass. *J. Geophys. Res.*, **104**, 1455–1464, <https://doi.org/10.1029/1998JC900022>.
- Kumar, V., P. K. Pradhan, T. Sinha, S. V. B. Rao, and H.-P. Chang, 2020: Interaction of a low-pressure system, an off-shore trough, and mid-tropospheric dry air intrusion: The Kerala Flood of August 2018. *Atmosphere*, **11**, 740, <https://doi.org/10.3390/atmos11070740>.
- L'Hégaret, P., L. Lacour, X. Carton, G. Roullet, R. Baraille, and S. Correard, 2013: A seasonal dipolar eddy near Ras Al Hamra (Sea of Oman). *Ocean Dyn.*, **63**, 633–659, <https://doi.org/10.1007/s10236-013-0616-2>.
- Large, W. G., J. C. McWilliams, and S. C. Doney, 1994: Oceanic vertical mixing: A review and a model with a nonlocal boundary layer parameterization. *Rev. Geophys.*, **32**, 363–403, <https://doi.org/10.1029/94RG01872>.
- Metzger, E. J., O. M. Smedstad, P. G. Thoppil, H. E. Hurlburt, D. S. Franklin, G. Peggion, J. F. Shriver, and A. J. Wallcraft, 2010: Validation test report for the Global Ocean Forecast System V3.0 – 1/12° YCOM/NCODA: Phase II. NRL Memo. Rep. NRL/MR/7320-10-9236, 76 pp.
- , and Coauthors, 2014: US Navy operational global ocean and Arctic ice prediction systems. *Oceanography*, **27**, 32–43, <https://doi.org/10.5670/oceanog.2014.66>.
- Morrison, J. M., 1997: Inter-monsoonal changes in the T-S properties of the near-surface waters of the northern Arabian Sea. *Geophys. Res. Lett.*, **24**, 2553–2556, <https://doi.org/10.1029/97GL01876>.
- Prasad, T. G., 1997: Annual and seasonal mean buoyancy fluxes for the tropical Indian Ocean. *Curr. Sci.*, **73**, 667–674.
- , and M. Ikeda, 2002a: The wintertime water mass formation in the northern Arabian Sea: A model study. *J. Phys. Oceanogr.*, **32**, 1028–1040, [https://doi.org/10.1175/1520-0485\(2002\)032<1028:TWWMF1>2.0.CO;2](https://doi.org/10.1175/1520-0485(2002)032<1028:TWWMF1>2.0.CO;2).
- , and —, 2002b: A numerical study of the seasonal variability of Arabian Sea high-salinity water. *J. Geophys. Res.*, **107**, 3197, <https://doi.org/10.1029/2001JC001139>.

- Ramesh Kumar, M. R., and T. G. Prasad, 1997: Annual and inter-annual variation of precipitation over the tropical Indian Ocean. *J. Geophys. Res.*, **102**, 18 519–18 527, <https://doi.org/10.1029/97JC00979>.
- Rochford, D. J., 1964: Salinity maxima in the upper 1000 meters of the northern Indian Ocean. *Aust. J. Mar. Freshwater Res.*, **15**, 1–24, <https://doi.org/10.1071/MF9640001>.
- Roxy, M. K., S. Ghosh, A. Pathak, R. Athulya, M. Mujumdar, R. Murtugudde, P. Terray, and M. Rajeevan, 2017: A threefold rise in widespread extreme rain events over central India. *Nat. Commun.*, **8**, 708, <https://doi.org/10.1038/s41467-017-00744-9>.
- Saha, S., and Coauthors, 2010: The NCEP Climate Forecast System Reanalysis. *Bull. Amer. Meteor. Soc.*, **91**, 1015–1058, <https://doi.org/10.1175/2010BAMS3001.1>.
- Schott, F., and J. P. McCreary, 2001: The monsoon circulation in the Indian Ocean. *Prog. Oceanogr.*, **51**, 1–123, [https://doi.org/10.1016/S0079-6611\(01\)00083-0](https://doi.org/10.1016/S0079-6611(01)00083-0).
- Shetye, S. R., A. D. Gouveia, S. S. C. Shenoi, G. S. Michael, D. Sundar, A. M. Almeida, and K. Santanam, 1991: The coastal current off western India during the northeast monsoon. *Deep-Sea Res.*, **38**, 1517–1529, [https://doi.org/10.1016/0198-0149\(91\)90087-V](https://doi.org/10.1016/0198-0149(91)90087-V).
- Singh, S., V. Valsala, A. G. Prajeesh, and S. Balasubramanian, 2019: On the variability of Arabian Sea mixing and its energetics. *J. Geophys. Res. Oceans*, **124**, 7817–7836, <https://doi.org/10.1029/2019JC015334>.
- Wang, Z. K., S. F. DiMarco, A. E. Jochens, and S. Ingle, 2013: High salinity events in the northern Arabian Sea and Sea of Oman. *Deep-Sea Res. I*, **74**, 14–24, <https://doi.org/10.1016/j.dsr.2012.12.004>.
- Wyrtki, K., 1973: An equatorial jet in the Indian Ocean. *Science*, **181**, 262–264, <https://doi.org/10.1126/science.181.4096.262>.
- Zhang, Y., Y. Du, W. N. D. S. Jayarathna, Q. Sun, Y. Zhang, F. Yao, and M. Feng, 2020: A prolonged high-salinity event in the Northern Arabian Sea during 2014–17. *J. Phys. Oceanogr.*, **50**, 849–865, <https://doi.org/10.1175/JPO-D-19-0220.1>.